

## High-current perovskite solar cells fabricated with optically enhanced transparent conductive oxides

This content has been downloaded from IOPscience. Please scroll down to see the full text.

2017 Appl. Phys. Express 10 062301

(<http://iopscience.iop.org/1882-0786/10/6/062301>)

View [the table of contents for this issue](#), or go to the [journal homepage](#) for more

Download details:

IP Address: 210.212.129.125

This content was downloaded on 03/07/2017 at 06:03

Please note that [terms and conditions apply](#).

You may also be interested in:

[Enhanced optoelectronic quality of perovskite films with excess CH<sub>3</sub>NH<sub>3</sub>I for high-efficiency solar cells in ambient air](#)

Yunhai Zhang, Huiru Lv, Can Cui et al.

[Simulation of current–voltage curves for inverted planar structure perovskite solar cells using equivalent circuit model with inductance](#)

Ludmila Cojocar, Satoshi Uchida, Piyankarage V. V. Jayaweera et al.

[Effects of annealing rate and morphology of sol–gel derived ZnO on the performance of inverted polymer solar cells](#)

Yu Xuan, Hu Zi-Yang, Huang Zhen-Hua et al.

[Enhanced photovoltaic performance of planar perovskite solar cells fabricated in ambient air by solvent annealing treatment method](#)

Vincent Obiozo Eze and Tatsuo Mori

[Halide Perovskite Solar Cells Using Monocrystalline TiO<sub>2</sub> Nanorod Arrays as Electron Transport Layers: Impact of Nanorod Morphology](#)

Ujwal Kumar Thakur, Abdelrahman M Askar, Ryan Kisslinger et al.

[Towards optical optimization of planar monolithic perovskite/silicon-heterojunction tandem solar cells](#)

Steve Albrecht, Michael Saliba, Juan-Pablo Correa-Baena et al.



## High-current perovskite solar cells fabricated with optically enhanced transparent conductive oxides

Ryota Mishima\*, Masashi Hino, Hisashi Uzu, Tomomi Meguro, and Kenji Yamamoto

Kaneka Corporation, Settsu, Osaka 566-0072, Japan

\*E-mail: Ryota.Mishima@kaneka.co.jp

Received March 14, 2017; accepted April 21, 2017; published online May 15, 2017

We focused on fluorine tin oxide (FTO)-coated glass substrates for perovskite solar cells (PVSCs) and studied the effects of the optical properties and surface morphology on the short-circuit current density ( $J_{sc}$ ). The PVSC on our FTO substrate demonstrated a gain in  $J_{sc}$  by 1.4–1.6 mA/cm<sup>2</sup>, compared with the PVSCs on commercial FTO substrates. This is attributed not only to the low absorption of the FTO substrate but also to the suppression of reflection loss, caused by the light trapping effect on the textured surface. Finally, the power conversion efficiency of our PVSC reached >21% with less hysteresis. © 2017 The Japan Society of Applied Physics

Organic–inorganic hybrid perovskite solar cells (PVSCs) have attracted enormous interest because of their great promise of a low-cost manufacturing process.<sup>1)</sup> Hybrid perovskite materials possess good advantages such as high absorption coefficients, suitable direct band gaps, small exciton binding energies, and large diffusion lengths.<sup>2,3)</sup> Since Kojima et al. first reported perovskite-based dye-sensitized solar cells, rapid progress has been achieved in improving the photovoltaic performance of PVSCs.<sup>4)</sup> To date, the power conversion efficiency (PCE) has reached 22.1% in an active area of 0.09 cm<sup>2</sup>.<sup>5)</sup>

Most researchers have focused on fabrication techniques for perovskite thin films,<sup>6–8)</sup> the composition of perovskite materials,<sup>9–12)</sup> and the synthesis of new carrier transport layers,<sup>13–15)</sup> such as hole transport layers (HTLs) and electron transport layers (ETLs), in order to improve the PCE and reliability. A transparent conductive oxide (TCO) substrate is also considered to be one of the most important factors for determining device characteristics in the field of thin-film solar cells such as amorphous silicon and polymer solar cells; however, few reports of PVSCs have focused on TCO substrates.<sup>16)</sup>

It is of interest to understand the effects of the optical property and the surface morphology of the TCO substrate on the characteristics of the thin-film solar cells.<sup>17–19)</sup> In general, the device based on a highly textured TCO substrate exhibits a light trapping effect, such as the suppression of reflection loss and increased optical length, leading to the improvement of the short-circuit current density ( $J_{sc}$ ), compared with a device with a flat surface. On the other hand, current leakage often occurs owing to the insufficient coverage of films on the textured surface.

Fluorine tin oxide (FTO) is commonly used as the TCO substrate of PVSCs. Because of its outstanding heat properties, the physical properties of FTO can be maintained even when the substrate is heated at ~500 °C in the standard fabrication process of PVSCs. It is well known that the surface morphology of FTO can also be controlled by changing the deposition method. Therefore, it is important to understand the properties of FTO to maximize the device characteristics of PVSCs.

In this study, we demonstrated the improvement of  $J_{sc}$  by 1.4–1.6 mA/cm<sup>2</sup>, using the newly developed FTO substrate with the textured surface, in comparison with two other commercial FTO substrates. Because of the low absorption and light trapping effect of our substrate, the PVSC showed a PCE exceeding 21% with less hysteresis.

We prepared PVSCs by the fabrication method reported by Saliba et al.<sup>11)</sup> The device architecture is FTO/compact TiO<sub>2</sub> (c-TiO<sub>2</sub>)/mesoporous TiO<sub>2</sub> (m-TiO<sub>2</sub>)/perovskite/2,2',7,7'-tetrakis(*N,N*-di-*p*-methoxyphenylamino)-9,9'-spirobifluorene (Spiro-OMeTAD)/Au. The composition of perovskite is Cs<sub>10</sub>(MA<sub>0.17</sub>FA<sub>0.83</sub>)<sub>90</sub>Pb(I<sub>0.83</sub>Br<sub>0.17</sub>). On the basis of their method, the TiCl<sub>4</sub> treatment on the c-TiO<sub>2</sub> surface and the ultraviolet (UV)–ozone exposure prior to the deposition of a perovskite layer are achieved. The TiCl<sub>4</sub> treatment is reported by other research groups.<sup>20,21)</sup>

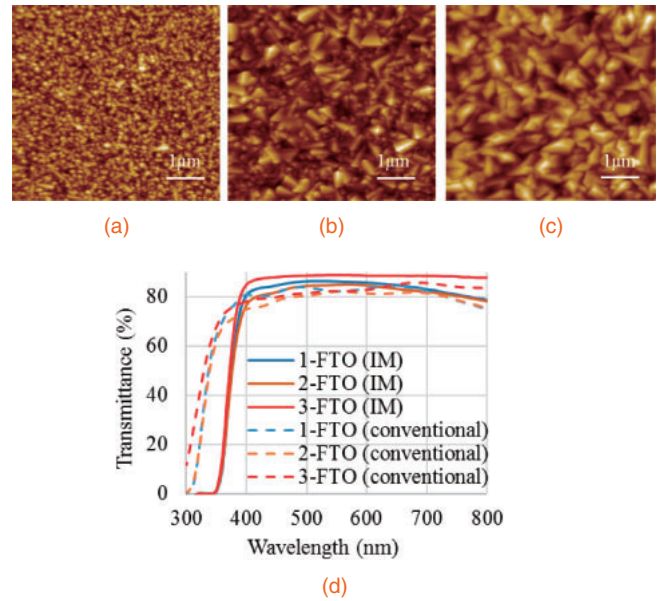
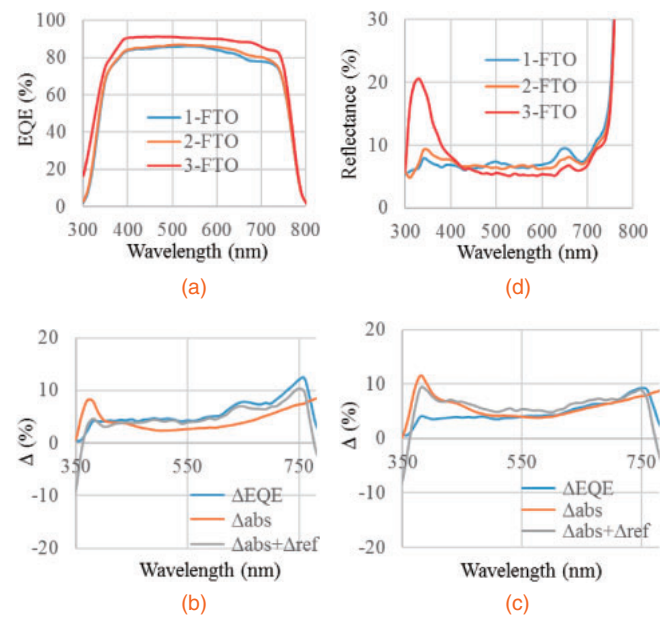
Three types of FTO-coated glass substrates were chosen to understand the effects of FTO properties on device characteristics. 1-FTO and 2-FTO were commercial substrates (Pilkinton TEC13 and TEC7), while 3-FTO was our newly developed substrate. The FTO-coated glasses were sequentially cleaned using detergent, acetone, and ethanol. A 20-nm-thick c-TiO<sub>2</sub> layer was deposited as the ETL on the cleaned FTO by spray pyrolysis at 500 °C from a precursor solution of 0.3 ml of titanium diisopropoxide in 4 ml of ethanol. The substrates were immersed in TiCl<sub>4</sub> solution at 70 °C for 10 min and sintered at 500 °C for 30 min, leading to higher c-TiO<sub>2</sub> conductivity. A 150-nm-thick m-TiO<sub>2</sub> layer was coated on the substrates by spin coating at a speed of 5000 rpm for 30 s with a ramp-up rate of 1000 rpm/s, by casting a diluted solution of 18-nm-particle-size paste (Dyesol 18NR) in ethanol; the weight ratio of TiO<sub>2</sub> paste to ethanol is 15%. After spin coating, the substrates were immediately preheated on a hotplate at 100 °C for 30 min and then sintered at 500 °C for 60 min. The mixed perovskite solutions were deposited from a precursor solution containing FAI (1.05 M), PbI<sub>2</sub> (1.1 M), MABr (0.2 M), and PbBr<sub>2</sub> (0.2 M) in DMF : DMSO = 4 : 1 solution. Then, 1.5 M CsI in DMSO was added to the mixed perovskite solution to obtain a triple cation composition. Before coating the perovskite precursor, UV–ozone treatment was applied to make the surface hydrophilic, and the substrates were immediately transferred to a nitrogen-filled glove box. The perovskite film was deposited by spin coating in a two-step program at 1000 and 6000 rpm for 10 and 20 s, respectively. During the second step, 150 μm of chlorobenzene was drop-cast on the spinning substrate 5 s before the end of the program. The substrates were then annealed at 100 °C for 1 h. The HTL was spin-coated at 3000 rpm for 30 s using Spiro-OMeTAD solution (70 mM in chlorobenzene) with added bis(trifluoromethylsulfonyl)imide lithium salt, tris[2-(1*H*-pyrazol-1-yl)-4-*tert*-butylpyridine]-cobalt(III)tris[bis(trifluoromethylsulfonyl)imide], and 4-*tert*-butylpyridien. The

**Table I.** Basic properties of three FTO-coated glass substrates, and  $J_{sc}$  of PVSCs on each substrate obtained from EQE and  $I$ - $V$  measurements.

	Sheet resistance ( $\Omega$ /sq)	IM Trans. at 500 nm (%)	Haze (%)	RMS (nm)	$J_{sc}$ (EQE) ( $\text{mA}/\text{cm}^2$ )	$J_{sc}$ ( $I$ - $V$ ) ( $\text{mA}/\text{cm}^2$ )
1-FTO	13	86.3	0.5	13.8	20.9	21.2
2-FTO	7	84.5	5.0	28.2	21.1	21.3
3-FTO	10	88.7	12.5	36.3	22.5	22.6

substrates were then annealed at 70 °C for 30 min. Gold rear electrodes of 100 nm thickness were thermally evaporated on the HTLs with an area of  $4 \times 6.5 \text{ mm}^2$ . Finally, current-voltage ( $I$ - $V$ ) and external quantum efficiency (EQE) measurements were achieved with an aperture mask of  $3 \times 5 \text{ mm}^2$  (active area of  $0.15 \text{ cm}^2$ ) under the ambient condition. The  $I$ - $V$  measurement was taken using a source meter (Keithley 2611B) under AM 1.5G illumination at  $100 \text{ mW}/\text{cm}^2$ , with a 150 W xenon light source (Bunkoukeiki BSX-150LC). The light intensity was calibrated using a reference Si photodiode (Bunkoukeiki BS-500BK) before the measurement. The scan rate was fixed at 50 mV/s. The  $I$ - $V$  curve was first measured in a backward scan from +1.2 to -0.1 V, and subsequently, the measurement in a forward scan was also achieved from -0.1 to +1.2 V for the evaluation of hysteresis. The measured EQE was plotted as a function of the excitation wavelength using monochromatic light from a 300 W xenon lamp (Bunkoukeiki BSX-300LC) passing through a monochromator. A silicon diode with a well-defined spectral response was used as a reference.

First, we evaluated the basic properties of three FTO-coated glass substrates, as shown in Table I. The sheet resistances of 1-FTO, 2-FTO, and 3-FTO are 13, 7, and  $10 \Omega/\text{sq}$ , respectively. The surface morphology of the substrates is observed by atomic force microscopy (AFM), as shown in Figs. 1(a)–1(c). 3-FTO presents pyramid structures with a root mean square (RMS) roughness of 36.3 nm and a maximum pyramid height of 294 nm. On the other hand, there are small particles resulting in a small roughness of 13.8 nm on the surface of 1-FTO, and a pyramid structure is partially observed on 2-FTO. The haze parameters of 1-FTO, 2-FTO, and 3-FTO are 0.5, 5.0, and 12.5%, respectively. The haze parameter is consistent with the pyramid structure on the FTO surface, as reported previously.<sup>21)</sup> Figure 1(d) shows the transmittance spectrum of each substrate obtained by an immersion (IM) method. By attaching diiodomethane liquids, whose refractive index is close to that of FTO, to the FTO surface, the scattering caused by the surface morphology of TCO can be eliminated.<sup>19)</sup> Therefore, the differences between the transmittance spectra obtained by the IM method are derived from the absorption of each FTO substrate. It turns out that 3-FTO has a low absorption in the measurement range of the wavelength, while the absorption of 1-FTO at wavelengths shorter than 700 nm is slightly lower than that of 2-FTO. However, there exists no sensitivity of transmittance at 300–350 nm in the IM method, owing to the absorption loss of diiodomethane liquids. The optical properties at wavelengths of 300–350 nm can be obtained from the conventional transmittance spectra obtained without the use of diiodomethane liquids [Fig. 1(d)], although the scattering

**Fig. 1.** AFM images of the surfaces of (a) 1-FTO, (b) 2-FTO, and (c) 3-FTO. (d) Transmittance spectra of 1-FTO, 2-FTO, and 3-FTO obtained by IM method. Dashed lines show conventional transmittance spectra.**Fig. 2.** (a) EQE spectra of PVSCs fabricated on 1-FTO, 2-FTO, and 3-FTO.  $\Delta$ EQE,  $\Delta$ abs, and  $\Delta$ ref (b) between 1-FTO and 3-FTO, and (c) between 2-FTO and 3-FTO. (d) Reflection spectra of the PVSCs fabricated on 1-FTO, 2-FTO, and 3-FTO.

effect remains on the FTO surface. This finding indicates that, again, only 3-FTO has a low absorption at 300–350 nm.

Next, the EQE spectra of the PVSCs on three FTO substrates were measured to gain insight into the effect of TCO on  $J_{sc}$ . Figure 2(a) shows the EQE spectra of three devices. All devices present a photoresponse onset at approximately 800 nm, which is consistent with the bandgap edge of the perovskite material. The EQE of the 3-FTO-based PVSC is higher than those of the other two devices at all wavelengths between 300 and 800 nm. The EQE of the 2-FTO-based PVSC is slightly higher than that of the 1-FTO-based PVSC at 550–800 nm. As a result, the integrated  $J_{sc}$  values of the PVSCs on 1-FTO, 2-FTO, and 3-FTO, calculated from EQE,

are 20.9, 21.1, and 22.5 mA/cm<sup>2</sup>, respectively, indicating that the  $J_{sc}$  of the 3-FTO-based PVSC is higher than those of 1-FTO- and 2-FTO-based PVSCs by 1.6 and 1.4 mA/cm<sup>2</sup>, respectively. In order to verify the accuracy of our results calculated from EQE,  $J_{sc}$  was also measured under AM 1.5G illumination at 100 mW/cm<sup>2</sup> in the  $I$ - $V$  measurements. The  $J_{sc}$  values of the PVSCs on 1-FTO, 2-FTO, and 3-FTO were 21.2, 21.3, and 22.6 mA/cm<sup>2</sup>, respectively, as shown in Table I. This indicates that the values of  $J_{sc}$  obtained under EQE and  $I$ - $V$  measurement conditions are almost the same. One of the origins of the higher EQE in the 3-FTO-based PVSC is considered to be the low absorption of the substrate. This can be verified by comparing the absorption difference ( $\Delta_{abs}$ ) of the FTO substrates, as estimated from the transmittance spectra obtained by the IM method, to the difference in the EQE spectra ( $\Delta_{EQE}$ ).  $\Delta_{EQE}$  and  $\Delta_{abs}$  relative to 3-FTO are plotted in Figs. 2(b) and 2(c). The plots indicate that the  $\Delta_{EQE}$  values between 1-FTO- and 3-FTO-based PVSCs, and between 2-FTO- and 3-FTO-based PVSCs cannot be explained by only  $\Delta_{abs}$ .

Thus, the reflectance spectra of the PVSCs were also obtained to better understand the origin of the difference in EQE. As shown in Fig. 2(d), the reflectance of the 3-FTO-based PVSC is the highest among the three devices at wavelengths below 450 nm. This can be explained by the low absorption of 3-FTO in this region, which causes a higher reflectance. The same properties are observed at wavelengths above 750 nm. In addition, the intensities of reflectance spectra of the devices are lower in the order of 3-FTO, 2-FTO, and 1-FTO at wavelengths between 450 and 750 nm. The change in reflectance in this region is considered to originate from the textured surface of FTO, which indicates that a highly hazed surface leads to the suppression of reflection loss owing to a light trapping effect. The previous study also revealed that the gain of EQE in amorphous silicon solar cells at longer wavelengths is caused by the light trapping effect.<sup>10</sup> The difference in  $J_{sc}$  between 1-FTO- and 3-FTO-based PVSCs, and between 2-FTO- and 3-FTO-based PVSCs for light trapping is estimated to be 0.26 and 0.15 mA/cm<sup>2</sup>, respectively.

The difference between these reflectance spectra ( $\Delta_{ref}$ ) is added to  $\Delta_{abs}$  in Figs. 2(c) and 2(d) and the sum of the spectra ( $\Delta_{abs} + \Delta_{ref}$ ) is compared with  $\Delta_{EQE}$ . This shows a fair agreement with the  $\Delta_{EQE}$  values of 1-FTO and 3-FTO, and 2-FTO and 3-FTO, except for the discrepancy between 2-FTO and 3-FTO in the region of short wavelengths. The origin of the discrepancy is still unclear; however, it is thought to be derived from the difference in the crystallinity of perovskite layers, which affects the absorption properties.

Here, we report the device characteristics of the PVSC formed on the 3-FTO substrate with an antireflective coating on the glass surface. The  $I$ - $V$  measurements of the 3-FTO-based PVSC were carried out in the forward and backward directions at 50 mV/s, as shown in Fig. 3(a). The values given below are the maximum values measured after device fabrication. The  $I$ - $V$  parameters of the device are as follows:  $J_{sc} = 24.1$  mA/cm<sup>2</sup>, open-circuit voltage ( $V_{oc}$ ) = 1.15 V, fill factor (FF) = 77.3%, and PCE = 21.50% in the forward scan;  $J_{sc} = 24.1$  mA/cm<sup>2</sup>,  $V_{oc} = 1.15$  V, FF = 77.8%, and PCE = 21.53% in the backward scan (Table II). The PCE of 21.5% obtained in our device is compatible with that in a previous

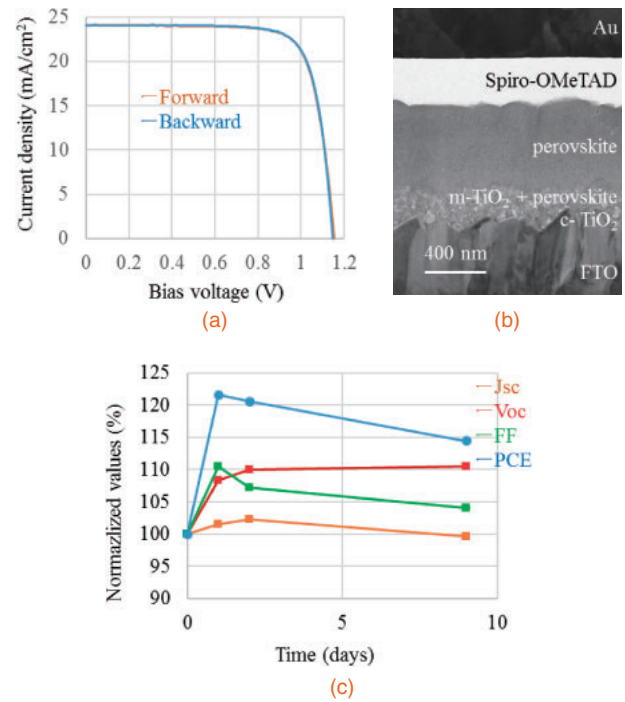


**Fig. 3.** (a)  $I$ - $V$  curves of the PVSC on 3-FTO measured in forward and backward scans. (b) Cross-sectional SEM image of the PVSC on 3-FTO. (c) Long-term stability of the 3-FTO-based PVSC after device fabrication.

**Table II.**  $I$ - $V$  parameters of the 3-FTO-based PVSC in forward and backward scans.

Scan direction	$J_{sc}$ (mA/cm <sup>2</sup> )	$V_{oc}$ (V)	FF (%)	PCE (%)	$R_s$ ( $\Omega$ cm <sup>2</sup> )	$R_{sh}$ ( $\Omega$ cm <sup>2</sup> )
Forward	24.1	1.15	77.3	21.50	3.1	4800
Backward	24.1	1.15	77.8	21.53	2.2	5250

paper.<sup>11</sup> There appears a significantly small hysteresis in our PVSC, as proven by  $J$ - $V$  curves shown in Fig. 3(a). Regardless of the scan direction, a  $J_{sc}$  of 24.1 mA/cm<sup>2</sup> is obtained, and  $V_{oc}$  also exceeds 1.15 V. Although the FFs in the two directions are also almost the same, there still exists a slight difference in series resistance ( $R_s$ ), which is associated with the favorable ionic movement in the perovskite layer, as pointed out in the previous paper.<sup>10</sup> The shunt resistance ( $R_{sh}$ ) values in both scan directions are so high that current leakage does not occur, even if the PVSC is formed on highly textured 3-FTO. This can also be confirmed in the cross-sectional scanning electron microscopy (SEM) image [Fig. 3(b)], which indicates the sufficient coverage of PVSC on 3-FTO.

Long-term stability is also an inevitable subject of PVSCs. Figure 3(c) shows time-dependent  $I$ - $V$  parameters of a bare cell within 9 d of device fabrication. The  $I$ - $V$  measurement was carried out under ambient conditions, and the device was stored inside a vacuum desiccator in the dark after measurement. Compared with the initial measurement, the increasing ratio of the PCE exceeds 20% after 1 d, particularly when  $V_{oc}$  and FF increased by  $\sim$ 10%. The time to reach the best PCE is dependent on the PVSCs themselves, although it is within a few days at most. Afterwards, the gradual decay of FF and  $J_{sc}$  occurs with  $V_{oc}$  remaining constant. Although the reason for this is still unclear, we believe that the highest PCE can be maintained by encapsulation in the near future.

In conclusion, we fabricated a PVSC on a newly developed FTO substrate and improved  $J_{sc}$  by 1.4–1.6 mA/cm<sup>2</sup> compared with other devices fabricated on commercially available FTO substrates. This improvement was attributed to not only the lower absorption of our FTO substrate but also the improved reflection loss. The PCE of the PVSC exhibited time dependence and reached up to 21% with less hysteresis approximately a few days after device fabrication.

**Acknowledgment** This work was supported in part by the New Energy and Industrial Technology Development Organization (NEDO) under the Ministry of Economy, Trade and Industry of Japan.

- 1) J. Seo, J. H. Noh, and S. I. Seok, *Acc. Chem. Res.* **49**, 562 (2016).
- 2) S. D. Stranks, G. E. Eperon, G. Grancini, C. Menelaou, M. J. P. Alcocer, T. Leijtens, L. M. Herz, A. Petrozza, and H. J. Snaith, *Science* **342**, 341 (2013).
- 3) G. Xing, N. Mathews, S. Sun, S. S. Lim, Y. M. Lam, M. Grätzel, S. Mhaisalkar, and T. C. Sum, *Science* **342**, 344 (2013).
- 4) A. Kojima, K. Teshima, Y. Shirai, and T. Miyasaka, *J. Am. Chem. Soc.* **131**, 6050 (2009).
- 5) M. A. Green, K. Emery, Y. Hishikawa, W. Warta, E. D. Dunlop, D. H. Levi, and A. W. Y. Ho-Baillie, *Prog. Photovoltaics* **25**, 3 (2017).
- 6) N. J. Jeon, J. H. Noh, Y. C. Kim, W. S. Yang, S. Ryu, and S. I. Seok, *Nat. Mater.* **13**, 897 (2014).
- 7) B. R. Sutherland, S. Hoogland, M. M. Adachi, P. Kanjanaboos, C. T. O. Wong, J. J. McDowell, J. Xu, O. Voznyy, Z. Ning, A. J. Houtepen, and E. H. Sargent, *Adv. Mater.* **27**, 53 (2015).
- 8) X. Li, D. Bi, C. Yi, J.-D. Décoppet, J. Luo, S. M. Zakeeruddin, A. Hagfeldt, and M. Grätzel, *Science* **353**, 58 (2016).
- 9) N. J. Jeon, J. H. Noh, W. S. Yang, Y. C. Kim, S. Ryu, J. Seo, and S. I. Seok, *Nature* **517**, 476 (2015).
- 10) J.-P. Correa-Baena, M. Anaya, G. Lozano, W. Tress, K. Domanski, M. Saliba, T. Matsui, T. J. Jacobsson, M. E. Calvo, A. Abate, M. Grätzel, H. Míguez, and A. Hagfeldt, *Adv. Mater.* **28**, 5031 (2016).
- 11) M. Saliba, T. Matsui, J.-Y. Seo, K. Domanski, J.-P. Correa-Baena, M. K. Nazeeruddin, S. M. Zakeeruddin, W. Tress, A. Abate, A. Hagfeldt, and M. Grätzel, *Energy Environ. Sci.* **9**, 1989 (2016).
- 12) M. Saliba, T. Matsui, K. Domanski, J.-Y. Seo, A. Ummadisingu, S. M. Zakeeruddin, J.-P. Correa-Baena, W. R. Tress, A. Abate, A. Hagfeldt, and M. Grätzel, *Science* **354**, 206 (2016).
- 13) W. Chen, Y. Wu, Y. Yue, J. Liu, W. Zhang, X. Yang, H. Chen, E. Bi, I. Ashraful, M. Grätzel, and L. Han, *Science* **350**, 944 (2015).
- 14) J. You, L. Meng, T.-B. Song, T.-F. Guo, Y. (M.) Yang, W.-H. Chang, Z. Hong, H. Chen, H. Zhou, Q. Chen, Y. Liu, N. D. Marco, and Y. Yang, *Nat. Nanotechnol.* **11**, 75 (2015).
- 15) M. Saliba, S. Orlandi, T. Matsui, S. Aghazada, M. Cavazzini, J.-P. Correa-Baena, P. Gao, R. Scopelliti, E. Mosconi, K.-H. Dahmen, F. D. Angelis, A. Hagfeldt, G. Pozzi, M. Grätzel, and M. K. Nazeeruddin, *Nat. Energy* **1**, 15017 (2016).
- 16) Z.-L. Tseng, C.-H. Chiang, and C.-G. Wu, *Sci. Rep.* **5**, 13211 (2015).
- 17) J. Müller, B. Rech, J. Springer, and M. Vanecek, *Sol. Energy* **77**, 917 (2004).
- 18) Z. Hu, J. Zhang, and Y. Zhao, *J. Appl. Phys.* **111**, 104516 (2012).
- 19) M. Isshiki, P. Sichanugrist, Y. Abe, T. Oyama, H. Odaka, and M. Konagai, *Curr. Appl. Phys.* **14**, 1813 (2014).
- 20) L. Cojocaru, S. Uchida, Y. Sanehira, J. Nakazaki, T. Kubo, and H. Segawa, *Chem. Lett.* **44**, 674 (2015).
- 21) Z. Liu, Q. Chen, Z. Hong, H. Zhou, X. Xu, N. De Marco, P. Sun, Z. Zhao, Y.-B. Cheng, and Y. Yang, *ACS Appl. Mater. Interfaces* **8**, 11076 (2016).